

letters

Conformation of the myosin motor during force generation in skeletal muscle

Malcolm Irving¹, Gabriella Piazzesi², Leonardo Lucii², Yin-Biao Sun¹, Jeffrey J. Harford¹, Ian M. Dobbie¹, Michael A. Ferenczi³, Massimo Reconditi² and Vincenzo Lombardi²

¹School of Biomedical Sciences, King's College London, New Hunt's House, Guy's Campus, London SE1 1UL, UK. ²Dipartimento di Scienze Fisiologiche, Università di Firenze, Viale GB Morgagni 63, I-50134, Firenze, Italy.

³National Institute for Medical Research, Mill Hill, London NW7 1AA, UK.

Myosin motors drive muscle contraction, cytokinesis and cell locomotion, and members of the myosin superfamily have been implicated in an increasingly diverse range of cell functions. Myosin can displace a bound actin filament several nanometers in a single interaction. Crystallographic studies suggest that this 'working stroke' involves bending of the myosin head between its light chain and catalytic domains. Here we used X-ray fiber diffraction to test the crystallographic model and measure the interdomain bending during force generation in an intact single muscle fiber. The observed bending has two components: an elastic distortion and an active rotation that generates force. The average bend of the force-generating myosin heads in a muscle fiber is intermediate between those in crystal structures with different bound nucleotides, and the C-terminus of the head is displaced by 7 nm along the actin filament axis compared with the *in vitro* conformation seen in the absence of nucleotide.

Myosins are characterized by a well-conserved catalytic domain (Fig. 1, red) that binds to the actin filament (gray, brown) and hydrolyzes ATP. A small 'converter' domain (green) links the catalytic domain to an extended light chain domain containing a long helical segment (blue) that binds calmodulin or the closely related myosin light chains (yellow, magenta)^{1–3}. The converter and light chain domains are thought to act together as a lever arm in the motor mechanism^{4–9}. The lower conformation in Fig. 1 (light blue long helix) shows the crystallographic structure of the catalytic, converter and light chain domains (referred to collectively as the myosin head) with no nucleotide in the active site¹ docked onto the actin filament using cryo-electron microscopy data⁴. The upper conformation (dark blue long helix) was calculated from the structure of a head fragment with the ADP•Pi analog, ADP•AlF₄⁻, in the active site⁸, under the assumption that the interface between the catalytic domain and actin is the same as in the nucleotide-free state. According to this model, release of ADP and Pi from the active site of myosin produces a working stroke that moves the tip of the lever arm 10.6 nm along the actin filament.

Testing the crystallographic model in a muscle fiber

In active muscle the myosin heads crosslink the actin and myosin filaments (Fig. 2a, gray and blue, respectively). The heads emerge from the myosin filament backbone with a regular 14.5 nm periodicity, giving rise to an intense X-ray reflection, called M3, which signals their conformation^{10–14}. The intensity of the M3 reflection (I_{M3}) was used to measure the bending angle between the light chain and catalytic domains. I_{M3} was calculated from the mass pro-



Fig. 1 Atomic model for the working stroke in the myosin motor. Gray/brown, actin filament; red, myosin catalytic domain (residues 1–707); green, converter domain (residues 711–781); blue, long helix (residues 781–843); yellow, essential light chain; magenta, regulatory light chain. The lower myosin structure (light blue long helix) shows skeletal muscle myosin¹ bound to actin in a conformation determined by cryo-electron microscopy in the absence of ATP⁴; the upper myosin structure is derived from a smooth muscle myosin fragment with ADP•AlF₄⁻ in the active site⁸. The catalytic domain of the ADP•AlF₄⁻ bound structure was superimposed on that of the nucleotide-free structure using residues 173–176, 187–199, 247–254, 262–268, 457–463 (root mean square deviation 0.057 nm); only the nucleotide-free catalytic domain is shown. The orientation of the light chain domain in the ADP•AlF₄⁻ structure was determined by superimposing residues 711–731 and 738–780 of the converter–light chain domain complex from the nucleotide-free structure onto the corresponding converter residues in the ADP•AlF₄⁻ bound structure, assuming that the converter–light chain complex moves as a rigid body^{7–9}. The M-line of the half-sarcomere is at the top. Residue numbers refer to chicken skeletal myosin. This figure was prepared with Molscript^{26,27} and Raster3D²⁸.

jections of the crystallographic structures onto the filament axis (Fig. 2b). I_{M3} for a general angle of interdomain bending is shown in Fig. 2c, where the horizontal axis shows the displacement (z) of the tip of the lever arm produced by the bending. The tip of the lever arm is also the junction between the myosin head and the rod domain which forms the backbone of the myosin filaments, so z can be related to the relative sliding between the myosin and actin filaments. $z = 0$ corresponds to the nucleotide-free structure (filled circle), which has a similar value of I_{M3} as the ADP•AlF₄⁻ structure ($z = 10.6$ nm; filled square). Intermediate bends give a larger I_{M3} , and the maximum value is at $z = 5.4$ nm, where the centroids of the lever arm and catalytic domains have the same axial coordinate, giving the narrowest axial density distribution (Fig. 2b).

We used X-ray fiber diffraction to test this model by measuring the changes in I_{M3} that accompany force generation in active single muscle fibers. We applied rapid length changes to the fibers to produce sliding between the actin and myosin filaments, and calculated the displacement of the myosin head–rod junctions (Δz) from the imposed filament sliding, taking into account the elasticity of the filaments^{14–17}. Then we compared the measured changes in I_{M3} and Δz with those expected from the crystallographic model (Fig. 2c). To make the tests of the model as definitive and demanding as possible, we improved the protocols used in previous fiber diffraction experiments^{11–14}. We used a time resolution of 100 μ s to eliminate the effects of myosin head detachment from actin, and devised multiple length step protocols in which filament sliding could either be imposed from the steady state of active isometric contraction or at the end of the working stroke.

Changes in M3 intensity produced by rapid length steps

An experimental protocol incorporating these features is shown in Fig. 3. Here a shortening step complete in ~ 150 μ s was

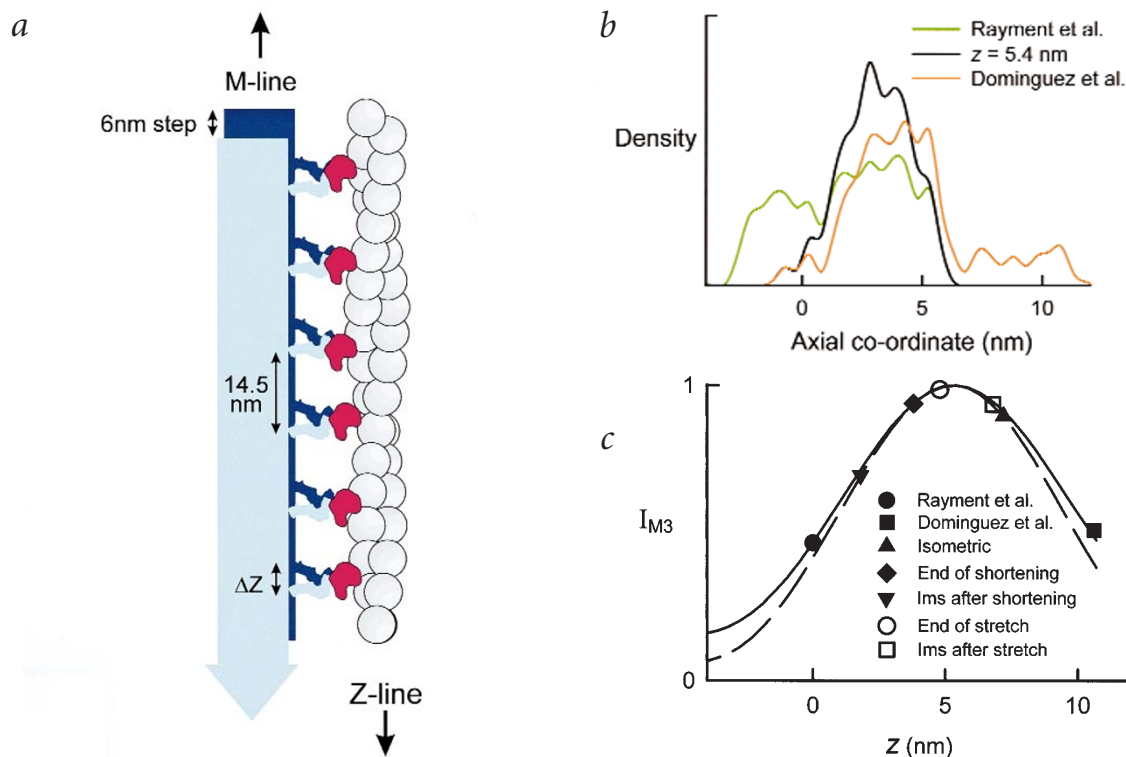


Fig. 2 Conformational changes in the myosin head produced by a length step in the muscle sarcomere. **a**, Actin filament, gray; myosin catalytic domain, red; myosin lever arm and filament, blue, with the lighter shade representing conformations after a shortening step Δz . **b**, Mass density distribution of the myosin heads projected onto the filament axis for the two crystallographic conformations in Fig. 1 and an intermediate conformation in which the displacement (z) of the myosin head-rod junction with respect to the nucleotide-free conformation⁴ was 5.4 nm. The axial co-ordinates of the catalytic domains have been superimposed and the zero denotes the axial co-ordinate of residue 843 in the nucleotide-free structure. **c**, Dependence of the intensity of the M3 X-ray reflection (I_{M3}) on z , with no conformational disorder (solid line; filled circle and filled square show the two crystallographic conformations), and for a Gaussian z dispersion of 2 nm (dashed line; filled triangles, filled diamond, open circle and open square correspond to five time points in the experiment in Fig. 3; see text for details).

imposed on an active muscle fiber, followed 1 ms later by a stretch of the same size. This length change cycle was repeated at 50 ms intervals, and the force produced by the fiber before each shortening step had the same value as the isometric force seen in the absence of length steps (superimposed traces in Fig. 3a). I_{M3} before the shortening step (Fig. 3d, filled circles) had the same value as in the absence of length steps (dashed line).

During the 150 μ s shortening step, the region of the muscle fiber illuminated by the X-ray beam shortened by 5.5 nm per half-sarcomere (hs) (Fig. 3b). The half-sarcomere is the fundamental functional unit of the muscle cell, comprising a set of myosin filaments anchored at the M-line overlapping with a set of actin filaments anchored at the Z-line (Fig. 2a). Thus each set of actin and myosin filaments slid together by a distance of 5.5 nm, and the measured force decreased from the value seen in the absence of applied length steps, called T_0 , to $0.25 T_0$ (Fig. 3c). On average, 2.1 nm of the imposed length change is taken up by filament elasticity ($0.75 T_0 \times$ the effective filament compliance^{14–17}, $2.8 \text{ nm } T_0^{-1}$), so the length perturbation at the myosin heads, Δz , was -3.4 nm. This produced little change in I_{M3} — at the end of the step I_{M3} was only $6 \pm 6\%$ (standard deviation, s.d.) larger than before it (Fig. 3d), suggesting that z had moved across the peak of the relation between I_{M3} and z (Fig. 2c). The mean change in I_{M3} was best fit with $z = 7.2$ nm before the step (filled triangle, Fig. 2c) and $z = 3.8$ nm after it (filled diamond, Fig. 2c).

In the 1 ms period after the shortening step, the force recovered to $0.66 T_0$ (Fig. 3c), as a result of the working stroke in the

actin-attached heads^{18,19}. This force increase re-extended the filaments by 1.1 nm, and each half-sarcomere shortened by 0.9 nm in the same period (Fig. 3b), so z decreased to 1.8 nm (Fig. 2c, filled inverted triangle). I_{M3} decreased during this period (Fig. 3d), as expected from the I_{M3} - z relation (Fig. 2c).

When a stretch was applied after the working stroke was largely complete, 1 ms after the shortening step, the force increased, then recovered towards its isometric value (Fig. 3c). The first few ms of this recovery are associated with the reversal of the working stroke²⁰. I_{M3} increased during the stretch (Fig. 3d), as expected for the change of z from 1.8 nm to 4.8 nm (open circle, Fig. 2c) on the steep ascending limb of the I_{M3} - z relation. There was little further change in I_{M3} during force recovery, as expected for the further increase of z to 6.8 nm (open square, Fig. 2c), across the peak of the I_{M3} - z relation.

Thus the crystallographic model reproduces the marked asymmetry between the synchronous I_{M3} response to stretch and the delayed response to shortening.

Myosin head detachment after length steps

One feature of the I_{M3} response in Fig. 3d (filled circles) is not predicted by the crystallographic model (open circles). I_{M3} in the period 1–5 ms after the stretch was $13 \pm 6\%$ (s.d.) less than its isometric value. The deficit is probably due to detachment of some of the myosin heads from actin, since detached heads make little contribution to I_{M3} in active muscle²¹. I_{M3} is already lower than expected 1 ms after the shortening step, so the detachment

letters

Fig. 3 Changes in force and the intensity of the M3 X-ray reflection (I_{M3}) produced by a shortening step and stretch separated by 1 ms during active contraction. **a**, Superimposed slow timebase force records in the presence and absence of the 40 length change cycles imposed at 50 ms intervals. Fiber cross-sectional area was $22,200 \mu\text{m}^2$ and its length was 6.75 mm ; the mean sarcomere length in the 2.10 mm segment was $2.09 \mu\text{m}$. Changes in **b**, segment length and **c**, force in the same fiber as part (a), sampled at $10 \mu\text{s}$ intervals, in the first part of the first length change cycle, and **d**, I_{M3} (filled circles, in $100 \mu\text{s}$ time bins) from 402 tetani in 14 fibers; the noise is predominantly due to the small number of diffracted X-ray photons in each time bin. The length change measured 1 ms after the start of the shortening step in these fibers was $6.36 \pm 1.12 \text{ nm hs}^{-1}$ (mean \pm s.d.). Dashed line: I_{M3} without applied length changes in the same fibers (48 tetani). Open circles were calculated from the dashed line in Fig. 2c with $z_{\text{iso}} = 7.2 \text{ nm}$.

rate may be faster than $1,000 \text{ s}^{-1}$. I_{M3} had fully recovered by the start of the next 50 ms cycle.

Measurements of sarcomere stiffness¹⁹ also suggest that some myosin heads detach from actin after a length step²². During a second length step applied 1 ms after a shortening step of $\sim 5 \text{ nm hs}^{-1}$, stiffness was $96 \pm 3\%$ (s.e. of mean, 6 fibers) of that in the first step. Allowing for filament compliance^{14,17}, the fraction of myosin heads attached to actin during the second step is $\sim 92\%$ of that in the first. Axial X-ray intensities are proportional to the square of the number of coherent diffractors, so I_{M3} should be reduced by $\sim 16\%$, similar to the observed deficit of 13% .

We conclude that detachment of myosin heads from actin after the shortening step can explain the I_{M3} deficit. The value of z , and thus the conformation of the myosin heads during isometric contraction is most reliably estimated from the change in I_{M3} during the first length step, when detachment is negligible¹⁹.

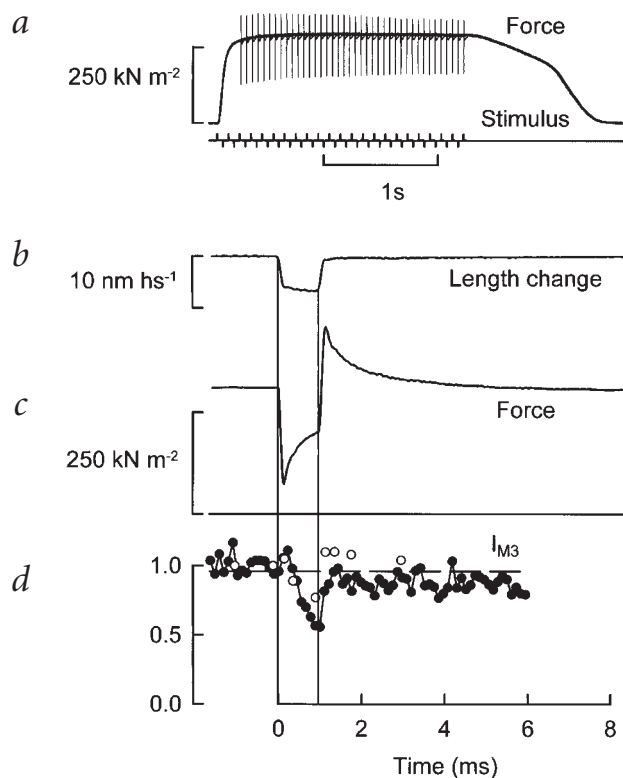
Myosin head conformation in isometric contraction

According to this criterion, the value of z during isometric contraction (z_{iso}) can be estimated as 7.2 nm from the experiment in Fig. 3. Another experiment, with $\Delta z = -2.2 \text{ nm}$, gave $z_{\text{iso}} = 7.4 \text{ nm}$. When a 5 nm stretch was imposed from the isometric state¹³, Δz was $+2.3 \text{ nm}$ and I_{M3} decreased by 25% , giving $z_{\text{iso}} = 6.2 \text{ nm}$. We conclude that z_{iso} is $\sim 7 \text{ nm}$. The isometric conformation of the myosin head is intermediate between the nucleotide-free ($z = 0$) and ADP \cdot Pi ($z = 10.6 \text{ nm}$) conformations in the crystallographic models.

This value of z_{iso} is an average over a distribution of head conformations with different bend angles between the light chain and catalytic domains. This distribution was modeled as a Gaussian distribution of z with a standard deviation of $\pm 2 \text{ nm}$, which is large enough to allow almost all the myosin heads to attach to actin, since an actin monomer is available every 5.5 nm along each strand of the actin filament. The normalized I_{M3} - z relation for this Gaussian distribution of z (Fig. 2c, dashed line) is similar to that in the absence of conformational disorder (solid line). Thus, the fractional change in I_{M3} is effectively independent of the conformational disorder that is likely to be present in the muscle fiber^{12,14}. Furthermore the present results are not consistent with a mixture of the two crystallographic conformations during isometric contraction, which would produce much smaller fractional changes of I_{M3} following length steps than those observed.

Double step experiments

As a critical test of the above approach and conclusions, we applied two shortening steps separated by 1 ms, but reduced the amplitude of the first to 2.5 nm hs^{-1} (Fig. 4). If z_{iso} is $\sim 7 \text{ nm}$, as we concluded in the previous section, then z should decrease from ~ 7 to $\sim 5 \text{ nm}$



after the first step. This should not produce much change in I_{M3} (Fig. 2c), but it should leave the myosin heads in a conformation where further shortening in the second step would produce a large decrease in I_{M3} . As expected, I_{M3} was roughly constant during the first shortening step and during the subsequent 1 ms of force recovery (filled circles, Fig. 4c). However I_{M3} decreased substantially during the second shortening step, in contrast to the response to a similar size shortening step from the isometric state (Fig. 3d), in which the I_{M3} decrease was delayed until the rapid force recovery phase. This difference in the kinetics of the I_{M3} response is also expected from the I_{M3} - z relation (open circles in Figs. 3d, 4c). The fiber was returned to its original length by sequential 6 and 2.5 nm stretches. Despite the low value of I_{M3} before the second 2.5 nm stretch, presumably due to detachment of some myosin heads from actin as discussed above, the second stretch produced no significant change in I_{M3} . This is also expected from the I_{M3} - z relation (open circles, Fig. 4c). Thus these double step experiments provide strong support for the isometric conformation of the myosin heads described in the previous section.

Structure-function relation of the myosin head

Bending of the myosin head and the corresponding changes in z have two functional components¹⁴. Active rotation of the lever arm is likely to be coupled to release of hydrolysis products from the active site (Fig. 1), but the myosin head is an elastic structure^{13,14}, and passive rotation of the lever arm may also occur in response to external stress. The structural basis of myosin head elasticity is unknown and we have analyzed the I_{M3} transients under the simplest assumption that both the passive and active rotations can be represented as bending between the lever arm and catalytic domain. The present approach cannot eliminate alternative possibilities, for example, an elastic element at the actin interface of the myosin head, or distributed along the lever

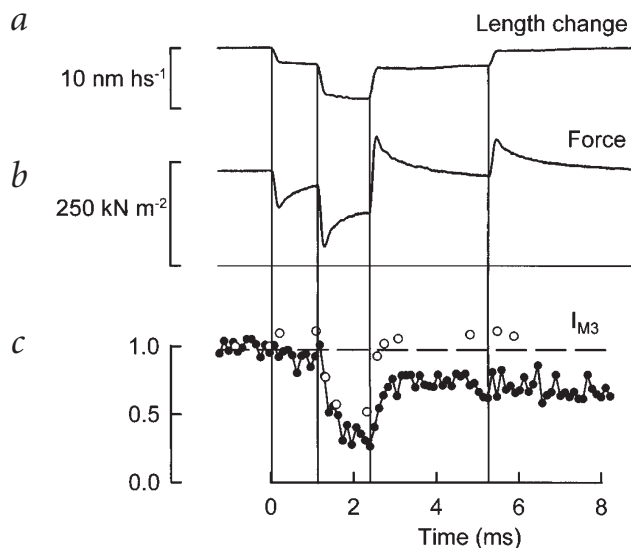


Fig. 4 Changes in force and the intensity of the M3 X-ray reflection (I_{M3}) in a double shortening step experiment. Changes in **a**, segment length, **b**, force and **c**, I_{M3} (filled circles) produced by a 2.5 nm hs^{-1} shortening step followed after 1 ms by a 6 nm hs^{-1} shortening step. X-ray data were collected from 207 tetani in six fibers; mechanical records were from a single fiber with a cross-sectional area of 16,300 μm^2 , length of 5.95 mm and a mean sarcomere length in the 2.47 mm segment of 2.10 μm . The length changes measured 1 ms after the start of the two shortening steps in the six fibers were 2.65 ± 0.26 and 5.73 ± 0.93 nm hs^{-1} , respectively (mean \pm s.d.). Dashed line: I_{M3} without applied length changes in the same fibers (14 tetani). Open circles were calculated from the dashed line in Fig. 2c with $z_{iso} = 7.2$ nm. Other conditions were as in Fig. 3.

arm¹⁴. The present conclusions are insensitive to the location of myosin head compliance.

The elasticity of the myosin head is central to our analysis, and has general functional significance in allowing force generation in the absence of filament sliding. The average elastic strain in the head during isometric contraction corresponds to an axial displacement of the head-rod junction by ~ 2.3 nm¹⁴. Consequently, of the total 7 nm displacement of the myosin head-rod junction between isometric contraction and the nucleotide-free state, ~ 5 nm is due to active tilting of the lever arm.

Methods

X-ray diffraction. X-ray measurements were made on single fibers from anterior tibialis muscles of *Rana temporaria*, at 4 °C, using station 16.1 of the CLRC Daresbury laboratory with a monochromator/mirror X-ray camera and two-dimensional gas-filled detector 3 m from the fiber²³. X-ray exposure was limited to data acquisition periods by a fast shutter. Detector output at 512×512 resolution was accumulated in 100 μs time bins in histogramming memory, with a 10 μs dead time between adjacent time bins. Data analysis used BSL and XOTOKO software provided by CLRC via Collaborative Computational Project 13 (CCP13). After correcting for detector response and camera background, the intensity of the M3 reflection (I_{M3}) was calculated by integrating the diffraction pattern between reciprocal spacings $1/53$ nm⁻¹ on either side of the meridian (parallel to the fiber axis) and fitting and subtracting a linear background between $1/17.0$ and $1/12.7$ nm⁻¹ along the meridian. There were no detectable changes in meridional or cross-meridional width of the reflection during the length changes.

Mechanical measurements. Mechanical measurements were made simultaneously on the same fibers used for the X-ray measurements^{12,24}. Length steps of ~ 0.15 ms duration were applied by a moving coil motor. Force was measured with a capacitance gauge transducer. The average sarcomere length in the ~ 2 mm segment of the fiber illuminated by the X-ray beam was recorded using a striation follower²⁵. Fibers were electrically stimulated for 2.3 s. After 0.3 s of stimulation at constant length, 40 shortening stretch cycles, each lasting ~ 50 ms, were imposed (Fig. 3a). The force before each shortening step was always the same as that in the absence of imposed length changes. Instantaneous force-sarcomere length relations were recorded with an 8 μs sample interval to minimize the effects of quick force recovery¹⁹. Changes in the fraction of myosin heads attached to actin, normalized by that during isometric contraction, were calculated from the measured stiffness assuming a filament compliance¹⁴ of 2.8 nm/ T_0 .

Calculation of I_{M3} from crystallographic models. I_{M3} was calculated from crystallographic models of the myosin head starting from the nucleotide-free conformation of the actin-bound head⁴, then allowing rotation of the lever arm with respect to the catalytic domain at residue 707. The lever arm (residues 707–843 of the heavy chain and both light chains) was assumed to move as a rigid body (Fig. 1). I_{M3} for any given rotation angle of the lever arm was calculated from the $1/14.5$ nm⁻¹ Fourier component of the axial mass projection of the entire myosin head¹⁴ and expressed in terms of the axial displacement (z) of the myosin head-rod junction (residue 843) with respect to the nucleotide-free structure (Fig. 2c). The observed fractional change in I_{M3} was compared with that expected from Fig. 2c using Δz calculated from the imposed filament sliding and force changes as described in the text. The only free parameter was the initial value of z during isometric contraction (z_{iso}). The mismatch between axial periodicities of the actin and myosin filaments must produce some conformational disorder of the heads; this reduces the absolute value of I_{M3} but has little effect on the fractional change during rapid length steps (Fig. 2c) because the disorder is constant during the step¹⁴.

Acknowledgments

We thank the noncrystalline diffraction group at the CLRC Daresbury laboratory for experimental facilities, A. Aiazzi and M. Dolfi for skilled mechanical and electronic assistance, and the UK MRC, CNR, MURST and Telethon (Italy) for financial support.

Correspondence should be addressed to M.I. email: malcolm.iring@kcl.ac.uk

Received 21 January, 2000; accepted 10 April, 2000.

1. Rayment I. *et al. Science* **261**, 50–58 (1993).
2. Xie, X. *et al. Nature* **368**, 306–312 (1994).
3. Cope, T.V., Whisstock, J., Rayment, I. & Kendrick-Jones, J. *Structure* **4**, 969–987 (1996).
4. Rayment, I. *et al. Science* **261**, 58–65 (1993b).
5. Whittaker, M. *et al. Nature* **378**, 748–753 (1995).
6. Corrie, J.E.T. *et al. Nature* **400**, 425–430 (1999).
7. Geeves, M.A. & Holmes, K.C. *Annu. Rev. Biochem.* **68**, 687–728 (1999).
8. Dominguez, R., Freyzon, Y., Trybus, K.M., & Cohen, C. *Cell* **94**, 559–571 (1998).
9. Houdusse, A., Kalabokis, V.N., Himmel, D., Szent-Györgyi, A.G., & Cohen, C. *Cell* **97**, 459–470 (1999).
10. Huxley, H.E., Faruqi, A.R., Kress, M., Bordas, J., & Koch, M.H.J. *J. Mol. Biol.* **158**, 673–684 (1982).
11. Huxley, H.E. *et al. J. Mol. Biol.* **169**, 469–506 (1983).
12. Irving, M., Lombardi, V., Piazzesi, G., & Ferenczi, M.A. *Nature* **357**, 156–158 (1992).
13. Lombardi, V. *et al. Nature* **374**, 553–555 (1995).
14. Dobbie, I. *et al. Nature* **396**, 383–387 (1998).
15. Huxley, H.E., Stewart, A., Sosa, H., & Irving, T. *Biophys. J.* **67**, 2411–2421 (1994).
16. Wakabayashi, K. *et al. Biophys. J.* **67**, 2422–2435 (1994).
17. Linari, M. *et al. Biophys. J.* **74**, 2459–2473 (1998).
18. Huxley, A.F. & Simmons, R.M. *Nature* **233**, 533–538 (1971).
19. Ford, L.E., Huxley, A.F., & Simmons, R.M. *J. Physiol.* **269**, 441–515 (1977).
20. Piazzesi, G., Linari, M., Reconditi, M., Vanzi, F. & Lombardi, V. *J. Physiol.* **498**, 3–15 (1997).
21. Piazzesi, G. *et al. J. Physiol.* **514**, 305–312 (1999).
22. Lombardi, V., Piazzesi, G. & Linari, M. *Nature* **355**, 638–641 (1992).
23. Towns-Andrews, E. *et al. Rev. Sci. Instrum.* **60**, 2346–2349 (1989).
24. Lombardi, V. & Piazzesi, G. *J. Physiol.* **431**, 141–171 (1990).
25. Huxley, A.F., Lombardi, V. & Peachey, L.D. *J. Physiol.* **317**, 12P–13P (1981).
26. Kraulis, P.J. *J. Appl. Crystallogr.* **24**, 946–950 (1991).
27. Esnouf, R.M. *J. Mol. Graph.* **15**, 133–138 (1997).
28. Merritt, E.A., & Bacon, D.J. *Methods Enzymol.* **277**, 595–524 (1997).